Published in final edited form as:
Sci Transl Med. 2023 August 02; 15(707): eadf2059. doi:10.1126/scitranslmed.adf2059.

Alternative splicing of CEACAM1 by Hypoxia-Inducible Factor–1α enhances tolerance to hepatic ischemia in mice and humans

Kenneth J. Dery[1], **Hidenobu Kojima**[1], **Shoichi Kageyama**[1,#], **Kentaro Kadono**[1,#], **Hirofumi Hirao**[1], **Brian Cheng**[1], **Yuan Zhai**[1,&], **Douglas G. Farmer**[1], **Fady M. Kaldas**[1], **Xiaoyi Yuan**[2], **Holger K. Eltzschiasg**[2], **Jerzy W. Kupiec-Weglinski**[1,*]

[1]The Dumont-UCLA Transplantation Center, Department of Surgery, Division of Liver and Pancreas Transplantation; David Geffen School of Medicine at UCLA, Los Angeles, CA, 90095 USA

[2]Department of Anesthesiology, McGovern Medical School at UTHealth; Houston, TX, 77030 USA

Abstract

Although alternative splicing (AS) drives transcriptional responses and cellular adaptation to environmental stresses, its contributions in organ transplantation have not been appreciated. We have shown that carcinoembryonic antigen-related cell adhesion molecule (Ceacam1; *CD66a*), a transmembrane biliary glycoprotein expressed in epithelial, endothelial, and immune cells, determines donor liver transplant quality. Here, we studied how AS of *Ceacam1* affects ischemia-reperfusion injury (IRI) in mouse and human livers. We found that the short cytoplasmic isoform *Ceacam1-S* increased during early acute and late resolution phases of warm IRI injury in mice. Transfection of Ceacam1-deficient mouse hepatocytes with adenoviral Ceacam1-S mitigated hypoxia-induced loss of cellular adhesion by repressing the Ask1/p-p38 cell death pathway. Nucleic-acid blocking morpholinos, designed to selectively induce Ceacam1-S, protected hepatocyte cultures against temperature-induced stress in vitro. Luciferase and chromatin

*Corresponding author. jkupiec@mednet.ucla.edu.
#Current address: Division of Hepato-Biliary-Pancreatic Surgery and Transplantation, Department of Surgery, Graduate School of Medicine, Kyoto University, Kyoto, 606-8501 Japan
&Current address: The Lee Patterson Allen Transplant Immunobiology Laboratory, Medical University of South Carolina, Charleston, SC 29415, UCLA

Author contributions: Conceptualization: KJD, YZ, XY, JWKW. Methodology: KJD; Investigation: KJD, HK, KK, HH, BC; Surgical procedures: HK, FK, SK; Clinical data analyses: FK, KJD, KK; Writing – original draft: KJD, JWKW; Writing – review & editing: KJD, YZ, HKE, JWKW; Project Administration: DGF, JWKW.

Competing interests: All authors declare that they have no competing interests and have not participated in consultation work related to this project.

List of Supplementary Materials
Materials and Methods
Fig. S1–S5.
Tables S1A–S2.
References: 13, 18, 61–70
Data File S1
MDAR Reproducibility Checklist

immunoprecipitation assays identified direct binding of hypoxia-inducible factor-1α (Hif-1α) to the mouse polypyrimidine tract binding protein 1 (*Ptbp1*) promoter region. Dimethyloxalylglycine (DMOG) protected mouse livers from warm IR-stress and hepatocellular damage by inhibiting prolyl hydroxylase domain-containing protein 1 (Phd1) and promoting AS of *Ceacam1-S*. Lastly, analysis of forty-six human donor liver grafts revealed that *CEACAM1-S* positively correlated with pre-transplant *HIF1A* expression. This also correlated with better transplant outcomes, including reduced *TIMP1*, total bilirubin, proinflammatory *MCP1*, *CXCL10* cytokines, immune activation markers *IL17A,* and incidence of delayed complications from biliary anastomosis. This translational study identified mouse Hif-1α-controlled AS of *Ceacam1*, through transcriptional regulation of *Ptbp1* promoter region, as a functional underpinning of hepatoprotection against IR-stress and tissue damage in liver transplantation.

One Sentence Summary:

HIF-1α-dependent alternative splicing of CEACAM1 is an essential regulatory mechanism for ischemic stress resistance in liver transplantation.

Editor's summary:

Recent evidence has suggested that the glycoprotein CEACAM1 is protective against ischemia-reperfusion injury during liver transplantation, but the specific contribution of each of its isoforms is not clear. Here Dery *et al* found that increased expression of the short cytoplasmic form of CEACAM1 (CEACAM1-S) limited hepatocyte injury and improved liver function in mouse models of acute liver injury. Further, CEACAM1-S was selectively increased through PTBP1- and HIF-1α-dependent alternative splicing. In humans, *CEACAM1-S* mRNA expression in donor livers before transplant correlated with improved liver function and transplant outcomes in recipients. These results suggest that CEACAM1-S may be a potential marker of liver quality and that efforts to increase its expression may have therapeutic benefits for transplantation or acute liver injury.

INTRODUCTION

Alternative splicing (AS) plays an important role in the transcriptional regulation of in vivo responses to environmental stressors. It increases the number of functional transcripts derived from the genome, and its regulation is required to direct cell development/differentiation (1). Through a series of well-coordinated events, splice site pairing occurs between the pre-mRNA and spliceosome, recognizing the variable exon (expressed) and intron (intervening) sequence. Modulating the usage of alternative exons depends on RNA-binding splicing regulators, where the heterogeneous nuclear ribonucleoproteins (hnRNPs) are among the prominent members (2). Considering their diversity/complexity, hnRNPs function in exon-definition, mRNA stability, and translational regulation (3), establishing themselves as essential proteins in cellular nucleic acid metabolism. Microarray data suggest that the human liver has the most divergent hnRNP expression program, likely due to the high frequency of genes (~35–40%) that express alternative exons (4). Although using high-throughput arrays and RNA sequencing has allowed for an unbiased assessment of

cellular AS, the biological function of alternatively spliced mRNAs in organ transplantation remains unknown.

Orthotopic liver transplantation (OLT) is a life-saving therapy of choice for end-stage liver diseases and certain hepatocellular malignancies (5). However, peri-transplant events, such as donor brain death, ischemia/reperfusion injury (IRI), and surgical trauma, cause the release of graft-derived damage-associated molecular patterns (DAMPs) that activate the recipient's innate immune response and negatively affect outcomes. In this context, there are critical gaps in our knowledge of molecular mechanisms regulating innate immune-driven sterile hepatic inflammation, and identifying non-invasive biomarkers that can predict OLT outcomes.

Our group recently discovered a checkpoint regulator of sterile IRI-inflammation in both mouse and human OLT (6). Activation of hepatic carcinoembryonic antigen-related cell adhesion molecule 1 (huCEACAM1; muCeacam1; *CD66a*), a transmembrane biliary glycoprotein expressed in epithelial, endothelial, and immune cells, was shown to affect donor liver quality, and prevent early OLT injury by suppressing the Ask1/p-p38 cell death pathway. It is well established that *CEACAM1/Ceacam1* undergoes extensive AS to generate two functionally distinct splice isoforms that lead to the exclusion or inclusion of a variable exon 7 (7–9). Splicing factors, such as hnRNP L and hnRNP A1, control splice-site recognition of exon 7 to form CEACAM1-L in breast cancer models (7, 8). Each variant shares identical amino acids in the N-terminal and transmembrane domain, differing at their cytoplasmic tail (10). The CEACAM1-S variant (for its short 12 amino acid tail) generally associates with epithelial cells and regulates mucosal immunity (11). In contrast, the CEACAM1-L (for its long >70+ amino acid tail) isoform inhibits signaling in myeloid and lymphocytic cells (12). *CEACAM1* mRNA is highly sensitive to environmental stress cues and can provoke epigenetic responses and control other AS programs (13). Indeed, CEACAM1 might act as a biosensor during hypoxia, because myocardial infarction in humans drives the expression of hypoxia-inducible transcription factors (HIFs) and regulates vascular endothelial growth factor (VEGF), which then leads to increased CEACAM1 expression (14). Another study found that hypoxic preconditioning of cardiomyocytes increased HIF-1α, VEGF, and CEACAM1 and ameliorated cardiac ischemic injury (15).

This study was designed to gain mechanistic insights into the role of *Ceacam1* alternative splicing in OLT. Our findings documented how specific induction of the Ceacam1-S variant during oxidative stress led to suppression of the Ask1 (Apoptosis signal-regulating kinase 1, a member of the MAP3K family) / p-p38 pathway and mitigated hepatocellular damage through HIF-1α transcriptional regulation of *Ptbp1* (polypyrimidine tract binding protein 1) expression. Stabilization of Hif-1α by dimethyloxalylglycine (DMOG) was indispensable for Ceacam1-S cytoprotection in vivo in two acute liver injury mouse models, lipopolysaccharide (LPS) and D-galactosamine (LPS/D-GalN)-induced hepatocellular damage, and warm hepatic IRI (wIRI). We also analyzed forty-six human OLT patients to determine the impact of AS of *CEACAM1* in the donor liver on phenotype and clinical outcomes and its relationship with *HIF1A*. Here, we provided evidence that liver graft-induced AS of *CEACAM1* mitigated IR-stress and promoted hepatic ischemia tolerance in OLT recipients.

RESULTS

Liver IRI promotes pre-mRNA AS of *Ceacam1*

First, we used a mouse model of hepatic wIRI to assess short cytoplasmic Ceacam1 isoform (Ceacam1-S) accumulation in the liver tissue after IR-stress. The peak of Ceacam1-S protein occurred at 6h after reperfusion, the height of hepatocellular damage in this model (Figs. 1, A and B) (16). At this time-point, Ceacam1-S expression was higher in the liver than in serum. Because it was unclear whether Ceacam1-S responded to acute inflammation during the ischemia insult vs. the resolution phase of IRI, we performed a longitudinal assessment over the course of 7 days to capture how *Ceacam1* isoform changes in both the acute and resolution phases of wIRI (Fig. 1C). The expression of *Ceacam1* mRNA was screened using exon-junction PCR amplification because this method allows alternative exons to be detected with high sensitivity. Notably, 6h and 7d time points showed peak AS induction of *Ceacam1*, documented by an increase in *Ceacam1-S* mRNA (Fig. 1D). When the hepatocellular damage (sAST) was assessed at 6h (Fig. 1E), it closely matched *Ceacam1-S* production (Sham vs. 6h, $P<0.0001$). These data suggest that Ceacam1 undergoes fine-tuning in response to IR-stress that might be functionally relevant.

Splicing variant Ceacam1-S but not Ceacam1-L limits hypoxic hepatocyte cold stress through repression of Ask1/p-p38 pathway

Our data so far hinted that the AS of *Ceacam1* might be important for limiting damage in IR-stressed livers. To document the role of each splicing isoform during hypoxic stress, we employed recombinant adenoviral (Ad) particles expressing Ceacam1-S or Ceacam1-L to transfect Ceacam1-deficient hepatocytes. First, after establishing the range of multiplicity of infection (MOI) of viral particles/cell (Fig. 2A), we observed viral-derived Ceacam1 proteins to be much higher than endogenous ones (Fig. 2, A and B). Grp78 (a master regulator of endoplasmic reticulum homeostasis) and not empty vector controls were used to show specificity (Fig. 2, A and B) while bright-field illumination microscopy analyzed Ceacam1's cellular adhesion properties in response to hypoxic stress. As expected, Ceacam1-deficient hepatocytes cultured under normoxic conditions showed loss of adhesion interface and structure compared to WT counterparts (Fig. 2C, top row, left vs. right), which was further exacerbated under hypoxic conditions. However, when cells were transfected with Ad: Ceacam1-S vs. Ad: Ceacam1-L, we observed only the short cytoplasmic Ceacam1 isoform rescued cell viability and promoted epithelial polarity maintenance, like WT cells (Fig. 2C, bottom row, left vs. right). Because previous studies showed that cold stress-conditioned Ceacam1-deficient hepatocytes experienced enhanced cell death in an Ask1-dependent manner (6), we now asked whether this mechanism was splice-isoform dependent. Ceacam1-deficient hepatocytes were first infected with diluted titers of viral particles to control for Ad-mediated cytotoxicity and then exposed to hypoxia and subsequent low temperature stress. Quantitation of immunoblots from these cells showed that as Ceacam1-S expression decreased (Fig. 2D, lanes 4 through 9 and Fig. 2E), Ask1 and p-p38 expression correspondingly decreased (Fig. 2E, $P=0.0177$, right panel), as compared to vector controls (Fig. 2D, lanes 1–3) and Ceacam1-L expression (Fig. 2D, lanes 10 through 15). This data implies that the AS of *Ceacam1* may be important in the mechanism of hepatic IRI. To test this hypothesis, WT mice were given isoform-specific Ceacam1

adenoviral particles (1×10^{11} viral particles/mouse i.v.) 24h before wIRI challenge. Serum ALT profiles showed that global overexpression of either Ad: Ceacam1 isoform did not ameliorate IRI (Fig. S1A, P=0.0300 Ad: Ceacam1-S vs. WT Cntl). Taken together with our liver/hepatocyte data so far, our data suggest induction of Ceacam1 alternative splicing in a tissue-specific manner may be a better approach to improve cell migration, proliferation, and survival following oxygen-stress.

Ceacam1-S splicing variant protects against temperature-induced hepatic stress in vitro

Organ preservation studies show that warm perfusion of previously cold-stored donor livers (with host blood) results in damage to hepatocytes and sinusoidal endothelial cells and Kupffer cell activation (17). Therefore, we next aimed to elucidate whether AS of *Ceacam1* promoted cytoprotection in temperature stress-inflicted hepatocyte damage. We designed splice-site blocking morpholino oligomers (MOs) to block the use of the exon 7 splice donor site, thereby shifting AS toward Ceacam1-S in WT hepatocytes (Fig. 3A). We used MOs directed to human E7 (E7: MO) that were previously described to produce the short isoform in HeLa cancer cells, presumably by disrupting RNA-protein interactions (8), or an exon-junction morpholino (EJ: MO) because thermodynamic profiling suggested a duplex of high stability.

Hepatocytes were then preconditioned with each MO and tested for *Ceacam1* mRNA AS under cold vs. warm stress conditions (Figs. 3B–3C). RT-PCR analysis revealed that while MOs induced AS equally well under cold stress (Fig. 3D, E7:MO (P<0.0001) and EJ:MO (P<0.0001) vs. NS:MO), EJ:MO targeting the 3’ splice site (ss) of exon 7 and 5’ ss of intron 7 performed better under warm stress than cold stress (Fig. 3D, 89.89% vs. 77.57%). AS alteration correlated with downregulation of Ceacam1-S protein in the cold storage (Figs. 3E–3F, 33.4% vs. 8.47%, P=0.0225, NS:MO vs. E7:MO), whereas warm storage led to the contrary (Figs. 3G–3H, P=0.0341). Hepatocyte “health” was monitored, as reported (18), using histone H3 expression, a well-known DAMP. Notably, loss of Ceacam1-S was correlated with enhanced histone H3 membrane leakage under cold stress (Figs. 3E–3F, P=0.0507, NS vs. EJ-MO), a measure of DAMPs activity. By contrast, we observed diminished Histone H3 release in hepatocytes under warm stress conditions (Figs. 3G–3H, P=0.1993 NS vs. EJ-MO Ceacam1). These in vitro findings led to the hypothesis that modulating hepatic Ceacam1 by systemic delivery of MOs (E7 or EJ) could potentially attenuate liver IRI in vivo (Fig. S1B). However, while sALT and sAST concentrations showed decreased enzyme levels with EJ:MO and more so with E7:MO, the difference was not statistically significant, as compared to WT controls, indicating that specifically biasing AS toward Ceacam1-S expression across parenchymal and nonparenchymal cells failed to alleviate hepatic IR-stress.

Hepatic Ceacam1-L exacerbates liver IRI and reduces OLT survival

Next, we tested the hypothesis that AS of *Ceacam1* plays an important role in hepatic IR damage in OLT recipients. Genetically-modified mouse donor livers, all from a C57BL/6 background, were subjected to extended cold storage (18h) and transplanted to syngeneic WT recipients (Fig. 4). Donors were divided into five groups, depending on whether in their livers Ceacam1 was present (WT), absent globally (GCC1-KO) or conditionally deficient

of CEACAM1-L (L-KO). The other two groups consisted of transgenic rat Ceacam1-L overexpressed in the C57BL/6 (CC1-Tg) or GCC1-KO (L-Resc) background (Fig. 4A). The hepatocellular function, assessed by sALT at 6h post-transplant, indicated that liver grafts expressing Ceacam1-L (CC1-Tg or L-Resc) did not do better than WT or GCC1-KO counterparts (Fig. 4B). When assessed at 14 days post-OLT, only conditional hepatic loss of Ceacam1-L (L-KO) led to improved overall survival (Fig. 4C), indicating the induction of alternatively spliced Ceacam1 is a necessary step in reducing IR-triggered hepatocellular damage in OLT recipients.

Control of AS of *Ceacam1* by Ptbp1 is dependent on oxygen availability

To focus on a molecular signaling pathway that underlies the control of hepatic AS during hypoxia, we next examined a known *CEACAM1* splicing regulator hnRNP A1 (8) and Ptbp1, using RNA interference. Ptbp1 was tested because its expression increases in rat pulmonary hypertension after hypoxia in a time-dependent manner (19). First, we confirmed that hypoxia induced a rapid and sustained accumulation of hnRNP A1 and Ptbp1 over time in primary mouse hepatocytes in vitro (Fig. S2A). Next, we showed that siRNAs efficiently silenced hnRNP A1 and Ptbp1 (Fig. S2B, P=0.0357 sihnRNP A1 vs. siControl). Then, Ceacam1-S protein expression was analyzed in the presence or absence of H/R (Fig. S2C). We found that the loss of these splicing factors increased expression of hepatic Ceacam1-L during hypoxia-reoxygenation stress, suggesting these RNA splicing factors may be involved in AS of Ceacam1-S in response to hypoxia (lanes 5, 7 vs. 3; measured as % E7 inclusion or Ceacam1-L, P=0.0022 sihnRNP A1 (siA1) ±H/R and P<0.0001 siPtbp1 (siP1) ±H/R).

Hif-1α promotes Ceacam1-S in vitro

Having established the role of AS of *Ceacam1* in H/R injury, we next sought to identify the factors that co-regulate transcription and hepatic *Ceacam1* splicing. HIF-1α has been suggested to modulate hypoxia-induced AS in tumor pathogenesis and progression (20). Since we observed a 6.7-fold (0.20/0.03) mean induction of Hif-1α in our liver wIRI model compared to Sham controls (Figs. 1B–1C, P=0.0324), we examined the role of Hif-1α in modulating AS of *Ceacam1* during hypoxia (Fig. 5A). We observed that hepatocytes exposed to less than 0.1% oxygen had substantial Hif-1α expression after hypoxia that decreased over time upon reoxygenation (Fig. 5B–5C). Hepatocyte cytotoxicity was monitored by assessing histone H3 and culture media AST concentrations (Figs. 5C–5D). Our data suggest that release of DAMPs may represent a hypoxic measure of acute early stress (Fig. 5B, lanes 3–4 and Fig. 5C, P=0.0197 0 h vs. Mock) whereas culture media AST concentrations may indicate how hepatocytes manage and recover from stress over the reoxygenation period (Fig. 5D). When the consequence on Ceacam1-S expression was monitored resulting solely from hypoxia, the effect was evident (Fig. 5B, lanes 2–4 vs. 1) but whether its kinetics followed Hif-1α's destabilization program during the progression towards normoxia was less clear (lanes 5 and 10 vs. 6–9).

To gain further insight into Hif-1α regulation of AS of *Ceacam1*, we employed a small molecule inhibitor (Echinomycin; Ecn) and stabilizer (cobalt chloride; CoCl2) of Hif-1α (Figs. 5E–5G). Ecn potently inhibited *Hif1A* gene expression at each concentration tested

(Fig. 5E, $P<0.0001$, 0 nM vs. 10 nM), and this correlated with transcriptional silencing of both *Ceacam1* isoforms (Fig. 5F, lanes 4–7 vs. 2–3; $P=0.0007$, 10 nM vs. Mock). With $CoCl_2$ stabilization of Hif-1α, we observed preferential induction of hepatic Ceacam1-S expression (Fig. 5G, lanes 3–4 vs. 2). Interestingly, Hif-1α stabilization also led to hepatic production of Ceacam1-L, albeit less efficiently than the Ceacam1-S isoform (magnified panel, Fig. 5G, lanes 5–7 vs. 2). To observe how Ceacam1-S and Hif-1α stabilization integrates intracellular responses from hypoxia, stressed hepatocytes were assessed by immunofluorescence staining (Fig. 5H). Our data shows punctate Hif-1α foci (green) in the nucleus correlates with the expression of Ceacam1 localization to the plasma membrane. Polarization of Hif-1α and Ceacam1 enhanced the cellular adhesion of stressed hepatocytes (red), though whether Hif-1α had a direct effect remained undetermined. This led to the hypothesis that Hif-1α may have the potential to influence pre-and post-transcriptional control of hepatic Ceacam1 under oxygen-rich and starved conditions.

Hif-1α associates with Ptbp1 under low oxygen conditions

We hypothesized that Hif-1α could control AS of *Ceacam1* by directly promoting the expression of RNA splicing factors hnRNP A1 and Ptbp1 through binding to HREs (hypoxia-responsive elements). To test this hypothesis, plasmid constructs containing approximately 1.2 Kb of WT *Ptbp1* or *hnRNP A1* promoter sequence were cloned upstream of a luciferase reporter (Fig. 6A). Mutations of *Ptbp1* (−900–537, −572–312 relative the TSS) and (−1805–1305) promoters to disrupt Hif-1α binding were also chosen based on computational in silico analyses (21). Transfected mouse hepatocytes co-cultured with WT *Ptbp1* and stressed with H/R showed the highest luminescence ($P=0.0041$) compared to the empty vector. Importantly, promoter mutations of *Ptbp1*, under similar H/R conditions, led to a significant luminescence decline (−900–537 vs. WT, $P=0.0082$ and −572–312 vs. WT, $P<0.0001$). By contrast, cells transfected with the WT *hnRNP A1* promoter did not appear to be responsive. Next, chromatin immunoprecipitation (ChIP) studies were performed to determine if the apparent regulation of *Ptbp1* by Hif-1α was the result of direct promoter interactions. SiRNA knockdown of Hif-1α in primary hepatocytes led to decreased Hif-1α expression (Figs. 6B–C, lanes 4–9, $P=0.0004$, siHif-1α vs. siCntl, +H) while loss of Hif-1α led to reduced Ceacam1-S (lanes 8–9 vs. 3, $P=0.0345$) and Ptbp1 (Fig. S3A–B, $P=0.0002$) expression. The specificity and sensitivity of the ChIP experiment were validated using anti-RNA polymerase II Abs and primers directed to positive control GAPDH (Fig. 6D). We also performed RT-PCR screening of the same *Ptbp1* promoter regions identified from our luciferase assay (Figs. 6E). We identified that Hif-1α binds to two HREs located in the promoter region of *Ptbp1* (Fig. 6F), one that is weakly induced by hypoxia (−900 to −537, $P=0.0002$, ± SEM 40.82 ± 3.292, ±H), and one that appears strongly hypoxia-dependent (−572 to −312, $P=0.0002$, ± SEM 280.0 ± 21.56, ±H). A summary of these induced interactions is shown in Fig. 6G.

DMOG Stabilizes Hepatic Hif-1α and Promotes Alternative Splicing to Alleviate Liver Injury

We next examined in vivo stabilization of Hif-1α by the prolyl hydroxylases (Phd) inhibitor, DMOG, as a way to alleviate liver injury. In the first of two animal models tested, DMOG was given before the co-administration of lipopolysaccharide and D-galactosamine (LPS/D-GalN) for 6h (Fig. S4A). This acute liver injury model provokes inflammatory

responses resembling hepatic fibrosis and causes genotoxic stress (22). Our data showed that hepatic mRNA expression of the anti-inflammatory cytokine *Il10* was highest after 1h pre-exposure to DMOG (Fig. S4B, P=0.0014, 1h vs. Sham), so we used this time point for further studies. Gross anatomical examination (Fig. S4C) showed that uncontrolled hemorrhaging, focal necrosis, and large areas of inflammatory cell infiltration evident by eye in control liver tissue were largely absent in DMOG-treated mice. Histological assessment of DMOG-treated hepatic tissue (Fig. S4D) exhibited decreased sinusoidal congestion, edema vacuolization, hepatocellular necrosis, and lower Suzuki's score of histological liver injury (Fig. S4E, P=0.0025, control vs. DMOG) compared to controls. The frequency of TUNEL-positive necrotic/apoptotic cells after DMOG treatment was significantly lower (Fig. S4F, P=0.0002 control vs. DMOG) as well as sALT concentrations (Fig. S4G) and proinflammatory mRNA coding for *Mcp1* and *Tnf* (Fig. S4H), all providing evidence that DMOG limited LPS/D-GalN-induced acute liver injury. Mice deficient of Ceacam1 (GCC1-KO) were then treated with vehicle or DMOG and compared to WT controls. Screening sALT concentrations showed that when Ceacam1 was absent, the protective effect of DMOG seen in WT was greatly diminished (Fig. S1C, P=0.0228).

We next asked whether exogenous DMOG administration was sufficient to induce AS changes in *Ceacam1* in vivo. Here, we used our wIRI model of sterile liver inflammation (Fig. 7A). Gross anatomical examination of control livers showed areas of red patches indicative of macrovesicular degeneration around hepatic cells (Fig. 7B). Elevated sAST and sALT, also reflected hepatocellular damage in the control mice as compared to the DMOG treatment group (Fig. 7C). In addition, liver tissue from DMOG mice showed histological evidence of reduced sinusoidal congestion, hepatocellular necrosis, and centrilobular ballooning as indicated by lower Suzuki's grading (Fig. 7D–E, P=0.0082 vs. Cntl). DMOG treated mice also had reduced frequency of TUNEL-positive cells (Fig. 7F, P<0.0001 vs. Cntl), elevated *Hif1A* and lower proinflammatory *Mcp1* mRNA compared to control injured mice (Fig. 7G). Since the initial stages of liver IRI involve the recruitment of circulating leukocytes, we next examined whether DMOG affected infiltrating Ly6G-positive neutrophils (Fig. 7H). Indeed, we observed little to no evidence that neutrophils were recruited to DMOG-preconditioned IR-stressed livers (Fig. 7I, P=0.0022, DMOG vs. Control). We confirmed by Western blots that PhD1 and Hif-1α showed reciprocal expression patterns with DMOG treatment (Fig. 7J). Control samples showed downregulation of Ceacam1-S at 6h post-reperfusion (Fig. 7K), whereas DMOG stabilization of Hif-1α led to an increase in Ceacam1-S protein. Analysis of *Ceacam1* mRNA isoforms also revealed a significant increase in exon 7 exclusion and *Ceacam1-S* mRNA in both control and DMOG-treated livers (Fig. 7M, P=0.0121, DMOG vs. Sham). Taken together, these data suggest that AS of *Ceacam1* occurs during acute hepatocellular injury and that DMOG can limit liver injury from IR-stress.

CEACAM1 expression before liver implantation associates with *HIF1A* in human OLT recipients

We next examined the hepatic *CEACAM1-S* expression in clinical OLT patients. Forty-six cold-stored human liver biopsies (Bx) were collected before graft implantation and analyzed (Fig. 8A). We found the correlation between total pre-transplant *CEACAM1-S* and *HIF1A*

mRNA was statistically significant (Fig. 8B, P=0.0034). We also divided pre-transplant human liver Bx samples into low vs. high *CEACAM1-S* expression groups, according to the median split method (cutoff=0.82) (Fig. 8C). Once again, we found *HIF1A* mRNA was significantly higher in livers with higher *CEACAM1-S* expression before transplant (Fig. 8D, P=0.0080, high vs. low). There was no correlation between *CEACAM1-S/ HIF1A* grouping and donor data (Table S1A), including age, gender, race, BMI, pre-transplant sAST, sALT, bilirubin, patient INR, or warm ischemia time. We also found no correlation between *CEACAM1-S/HIF1A* and the recipient or surgical parameters, including age, gender, race, BMI, disease etiology, ABO compatibility, MELD score (a measure of patient's liver disease severity), pre-transplant blood tests, pre-operative hospital stay, or cold ischemia time (Table S1B). We did, however, find lower post-transplant expression of *TIMP1*, a metalloproteinase inhibitor of integrin signaling in liver samples with high *CEACAM1-S* expression (Fig. 8E, P=0.0012, high vs. low). We also identified other important relationships with *CEACAM1-S* expression including post-OLT total bilirubin (Fig. 8F), delayed complications from biliary anastomosis, a surgical procedure for the management of biliary obstruction or post-OLT leakage (Fig. 8G, P=0.0223 delayed vs. non-delayed), and decreased mRNA expression of *MCP1*, *CXCL10* and *IL17A* post-OLT (Fig. 8H). We also examined pre-OLT expression of *CEACAM1-S* mRNA isoform in thirty-eight cold-stored livers and found its expression positively correlated with patient MELD scores (Fig. 8I), which may highlight CEACAM1's role as a stress response regulator in the high acuity livers. Bx samples were also subjected to classification of high vs. low expression groups, based on a median split method (cutoff=0.81, Fig. S5A). We found that pre-OLT *CEACAM1-S* also trended lower for incidence of surgical complications exceeding Grade III (Fig. S5B), sALT and sAST (Fig. S5C), post-OLT *CD80*, *CTLA4*, *CD68,* and *TIMP1* mRNA expression (Fig. S5D) as well as bilirubin (Fig. S5E), although the data failed to reach any statistical differences. Finally, Pearson r correlations analyzing pre-transplant *CEACAM1-S* vs. post-OLT *IL17A*, *TIM3*, and *CXCL10* mRNA showed negative trends (Fig. S5F).

DISCUSSION

This study originated as a follow-up to our recent report identifying Ceacam1 as a biomarker for donor graft quality in mouse and human OLT (6). Remaining unanswered was the genetic regulatory mechanisms by which hepatic Ceacam1 controls IR-stress and sterile inflammation (23). We have now identified a *Ceacam1* alternative splicing response to liver tissue stress or injury that appears to be Hif-1α dependent. Our data also suggest Ceacam1 signaling depends on the mechanisms that alter *Ceacam1* splicing regulation and not necessarily its overexpression.

To date, the effects of hypoxia on *Ceacam1* splicing isoforms remain conflicted. For instance, human dermal lymphatic endothelial cells exposed to hypoxic preconditioning downregulate CEACAM1 (24), whereas its expression in cardiac ischemic injury, increases along with other hypoxic angiogenic factors, such as HO-1 and HIF-1α (15). Here, we focused on *Ceacam1* splicing during the hepatic IRI cycle that occurs during liver transplantation (Fig 1). Our data revealed the AS of *Ceacam1* both in the early acute (6h) and late resolution (7d) phase of the hepatic IRI. Notably, we documented the mRNA

profiles in the stressed liver tissue and hepatocytes that parallel sAST concentrations in vivo and culture supernatants in vitro. These findings provide evidence that AS is regulated through endogenous cues and environmental post-reperfusion signals.

Each cytoplasmic domain of CEACAM1 is known to differ in length, ranging from 74-residue for CEACAM1-L to 12-residues for CEACAM1-S, and this feature determines their inhibitory or non-inhibitory signal transduction pathways (10). Although the cytoplasmic tail is minimal, the short cytoplasmic domain of CEACAM1-S can bind to actin, tropomyosin, annexin II and calmodulin (25, 26). Previous studies show that phosphorylation of key Thr and Ser residues in the short cytoplasmic domain (27, 28) promote the differentiation of vimentin-positive and β2-integrin-positive myofibroblasts (29), which is a critical step for the production of extracellular matrix (ECM) proteins in wound healing (30).

Modifications in ECM composition is also associated with reperfusion injury or acute and chronic rejection in human organ transplantation (31, 32). For example, the expression of fibronectin (FN) and laminin (LN) proteins increased rapidly in cardiac allo- and iso-transplant rat studies, reflecting a response to tissue ischemia during the initial stages of cardiac engraftment (33). FN expression arises due to AS of a single gene transcript composed of three segments, EIIIA, EIIIB, and V in rats (34), and associates with leukocytes. This was demonstrated when adoptively transferred sensitized lymphocytes localized in FN-rich areas of cardiac transplants and draining lymph nodes of test recipients (35). It will be important for future studies to determine whether Ceacam1 signaling, in its capacity to influence the ECM, has a similar regulatory function in integrin-mediated leukocyte adhesion in OLT.

The two major types of liver injury in the peri-transplant period involve warm and cold ischemia. Warm ischemia leads to delayed graft function, liver, or even multi-organ failure, with cellular changes including profound microcirculatory dysfunction, impaired vasodilatory capability, and endothelial activation, increased hepatic vascular resistance, liver inflammation, leukocyte infiltration, oxidative stress, and cell death (36). By contrast, cold IRI occurs during ex vivo preservation and is initiated by local inflammatory innate immune activation (37). Both types of IRI trigger liver Kupffer cells and neutrophils activation, cytokine and chemokine production, ROS generation, adhesion molecules induction and immune cell infiltration.

Our recent data showed that liver-resident total Ceacam1-S mitigated cold-induced early hepatocellular damage by suppressing the Ask1/p-p38 pathway (6), but which isoform was involved in this protective mechanism remained unclear. Ask1 acts as a redox-sensitive upstream activator of c-Jun N-terminal kinase (JNK) and p38 mitogen-activated protein kinases in response to stressors including oxidative stress, endoplasmic reticulum stress and calcium influx (38). Our previous data from an in vitro mimic model of warm/cold stressed primary hepatocytes revealed hepatocellular damage (18) comparable to ex vivo liver perfusion during OLT surgery. We now showed that forced conditional expression of Ad: Ceacam1-S but not Ad: Ceacam1-L attenuated stress responses in hypoxic and cold-stressed hepatocytes in vitro (Fig. 2), suggesting a protective role for Ceacam1-S. It will be interesting for future studies to investigate this molecular mechanism in more

detail, especially considering the short isoform's role in promoting apoptosis during lumen formation in the mammary ducts (39).

We were not able to observe a protective effect in our wIRI studies in vivo through adenoviral or morpholino mediated overexpression of Ceacam1-S. However, these proof-of-concept studies have highlighted the fact that forced expression of any one isoform across cell types may be detrimental and that, organ-specific delivery of morpholinos are needed to achieve therapeutic benefit. Studies using antisense oligonucleotides (ASOs) have shown efficacy in animal models in vivo (40) and two ASOs, fomivirsen (Vitravene) and mipomersen (Kynamro), developed by Isis Pharmaceuticals, are among the first to be approved by the US FDA for human clinical trials (41). Whether ASOs can manipulate CEACAM1 expression in human liver grafts to improve long-term clinical outcomes or be used to "rejuvenate" suboptimal donor livers during machine preservation before implantation awaits further study.

How AS of Ceacam1 influences the myriad of molecular functions deleterious for transplant outcomes remains unclear. Notably, our in vitro inflammation model showed strong induction of AS after oxygen-starvation, suggesting a role for HIF activity. Previous studies have shown that the α and β subunit interaction is more important for HIF activity than hypoxia stabilization *per se* to initiate AS regulation (42). Both α and β subunits form a heterodimer in the nucleus to induce transcriptional changes involved in the hypoxic response, affecting metabolism, angiogenesis, anti-apoptosis, and cell motility. Hypoxia inhibits oxygen-dependent oxygenases, such as HIF-dependent prolyl-hydroxylases (PHDs) (43). PHD inhibition leads to the accumulation, stabilization, and activation of HIF to initiate the transcriptional activation of HIF targets. Hypoxia also drives the expression of hypoxia-induced RNA binding protein ELAVL1 (embryonic lethal abnormal vision family of RNA-binding proteins, HuR), which modulates the expression of translation-initiating 4E nuclear import factor 1 (Eif4enif1) (42, 44), and HO-1, which mitigates hepatic IRI in OLT recipients (18). In ischemic heart disease, AS of calcium/calmodulin-dependent protein kinase II gamma, (CAMK2G), a crucial signaling molecule for adaptation of cardiac stress, is directly dependent on HIF-1α (45), suggesting Hif-1α may play a role in AS during hypoxic stress.

Our study showed that stabilization of Hif-1α with $CoCl_2$ strongly induced AS to express preferential Ceacam1-S and implicate Ptbp1 as an important splicing factor for modulating Ceacam1-S expression under hypoxic conditions. As oxygen tension increases, an adaptive response reorganizes the chromatin structures surrounding *Ptbp1* so that Hif-1α accessibility to HRE sites increases. Other HIF isoforms (HIF-2α and HIF-3α) also regulate hypoxia-inducible gene transcription (46) and may be essential in Ceacam1-S expression. Regulation of retinal neovascularization in patients with ischemic disease has been shown to depend on HIF-1α and HIF-2α (47). Therefore, future studies should also investigate the role of other HIF isoforms in the AS of downstream HIF targets in OLT.

We also examined the potential of pharmacologic interventions directly enhancing hepatic AS of Ceacam1 through DMOG, an inhibitor of PhD1, to increase HIF expression. Recent studies support these findings by showing that HIF-1α is a direct transcriptional suppressor

of interferon regulatory factors, specifically the transcriptional activators of type I IFN (48). Hypoxia-induced HIF-1α functions as a direct transcriptional repressor of IRF5 and IRF3. Interestingly, we previously showed that IRF3 and IRF7, both positive regulators of type I IFN gene induction downstream of pattern recognition, biases AS towards exon 7 inclusion to produce CEACAM1-L in human HeLa cancer cells (13). Although our DMOG data shows amelioration of liver IRI and induction of Hif-1α and Ceacam1-S expression, one limitation of our study is the inability to extend our findings regarding AS of other downstream HIF-targets, which was beyond the scope of this study. However, as approximately 95% of multi-exon human genes are alternatively spliced (49) and more than 70 direct HIF target genes are known to function in physiology and disease processes, including redox homeostasis/apoptosis (50), future studies may reveal additional important splicing events in OLT.

Currently, phase 2/3 clinical trials are testing the efficacy of HIF stabilizers in renal anemia (51). Previous studies have shown that DMOG plays a role in decreasing NADH, and coupled to glycolysis inhibitors, can deplete cellular ATP while increasing oxygen (52). As ATP is among the molecules released by cell damage, the use of DMOG during organ preservation to prevent positive feedback signaling by immune cells may be valuable. DAMPs released from damaged hepatocytes during IRI are detected by immune cells, and recruitment of other immune cells follows, which in turn facilitates neutrophil migration to a site of tissue injury. Whether University of Wisconsin (UW) solution, a gold standard for organ storage in transplantation, supplemented with DMOG during cold storage could reduce cellular ATP and prevent immune cascades that activate Kupffer cells and neutrophils await further studies. Although we recognize that DMOG may exert beneficial functions in a non-HIF-1α dependent manner (53), our findings reveal that DMOG regulates AS and inflammation and may serve as a starting point for the therapeutic development of hepatic IRI treatments in OLT recipients.

Our clinical data revealed the benefits of *HIF1A* and *CEACAM1-S* mRNA expression in OLT patients. High pre-OLT *HIF1A* and *CEACAM1-S* were correlated with lower *TIMP1* (Fig. 8E) in the post-reperfusion liver Bx samples. This metalloproteinase inhibitor has been shown to be under the regulation of CEACAM1 in a type 2 diabetes (54) and HIF-1α in a cancer model (55). A relationship between post-OLT total bilirubin and high pre-OLT *CEACAM1*/ *HIF1A* was also observed (Fig. 8F). The role of serum CEACAM1 in patients with hepatocellular carcinoma and total bilirubin has been described (56), along with how bilirubin induces *HIF1A* transcription (57). Whether DCD (donation after cardiac death) and/or pre-OLT donor tissue utilize these signaling pathways to resist cold storage awaits further studies. However, it is interesting to note that the bilirubin/ *CEACAM1*/ *HIF1A* relationship extends from pre-OLT to post-OLT outcomes and could represent a much-needed diagnostic bioassay for clinical outcomes. Fig. 8G also shows how pre-OLT *CEACAM1*/ *HIF1A* correlated with incidence of biliary-enteric anastomosis, a surgical procedure for the management of biliary obstruction or leakage after OLT. Post-OLT biliary complications include strictures (anastomotic and non-anastomotic), leaks, stones, sphincter of Oddi dysfunction, and recurrence of primary biliary disease, such as primary sclerosing cholangitis and primary biliary cirrhosis (58). Strikingly, our data showed no patients with

biliary anastomosis in the high *CEACAM1*/ *HIF1A* group, being another indicator for future OLT success.

Our study had some limitations. First, we focused largely on primary cultured hepatocytes without consideration of how resident cells, like Kupffer cells, or non-parenchymal liver cells (sinusoidal endothelial cells and stellate cells) may contribute. It will be interesting to test how ischemic stress affects *Ceacam1-S* in these cell types, which may provide additional insight to improve antisense MO or DMOG-based therapies. Second, as our liver transplant clinical data analyses focused on mRNA expression, future studies should evaluate the correlation between mRNA and protein levels. Third, as biological samples were collected in bulk for RNA and protein analyses, next-generation technologies such as single-cell RNA-seq should be conducted to fully appreciate the role that AS plays in IRI and provide the resolution for detailed characterization of treatment-induced differentiation pathways in vitro and in vivo. Fourth, we only tested the role of hypoxia-dependent stabilization of HIF-1 dimers, making the assumption that Hif-1α is the primary driver of various biological processes and functions, including cell survival, proliferation, and metabolism. Although our DMOG and $CoCl_2$ studies showed rapid stabilization of Hif-1α, focusing on one HIF alpha subunit only may have limited the overall efficacy of our experimental therapy. We cannot exclude the contribution of other HIF family members such as HIF-2α that may participate in AS, so further study will be needed to identify more specific HIFα subunit therapies. Fifth, we compared the role of AS in mouse *Ceacam1* to the relationship between human *HIF-1α* and *CEACAM1*. Future studies using transgenic mouse models of human CEACAM1 should ultimately strengthen comparisons to human liver transplant clinical cohorts. Finally, prospective clinical trials should be conducted to analyze therapeutic effects and better understand how the engagement of AS gene regulatory networks and their translation to relevant proteins can be exploited for targeting hepatic sterile inflammation in OLT recipients.

Of note, our recent molecular and functional studies have shown that despite neutrophils being considered a principal villain in peri transplant tissue injury, their Ceacam1-L isoform may repress neutrophil extracellular trap (NET) formation in IR-stress resistance in human and mouse OLT recipients (59). Indeed, by determining the susceptibility to NET formation via autophagy signaling, neutrophil Ceacam1-L isoform may serve as a biomarker of NETosis and a checkpoint regulator of sterile inflammation. Hence, our present and former studies highlight cell-specific “beneficial” functions of hepatocyte Ceacam1-S and neutrophil Ceacam1-L isoforms, and their crosstalk in the stressed liver tissue certainly warrants future in-depth assessment.

In conclusion, this translational study not only addresses how hepatic CEACAM1 acts as a checkpoint regulator of IR-stress and sterile inflammation in the liver, but also adds to the limited knowledge of how post-transcriptional regulatory machinery may affect OLT in mice and humans. Hif-1α contributed to *Ceacam1* AS through regulation of Ptbp1. Increased Ceacam1-S expression improved ischemia tolerance, suggesting that this mechanism may represent a potential therapeutic target for hepatoprotection against IR-stress in OLT.

MATERIALS AND METHODS

Study design

This study was designed to determine the functional role of AS of *Ceacam1* and its crosstalk with Hif-1α signaling in hepatic IR-stress and injury in mice (in vivo models of liver wIRI/OLT and in vitro models of primary hepatocyte cultures exposed to oxygen-stress conditions) and humans (forty-six adult primary OLT recipients). All mouse experiments were approved by the UCLA Animal Research Committee (ARC #1999–094). For mouse studies, daily monitoring was performed and if they became symptomatic (including an enlarged head, ataxia, or weight loss of up to 25%), individuals were euthanized. Mice were excluded when hydrocephalus was observed. All human studies were approved by the UCLA Institutional Research Board (IRB protocol 13–000143) and written informed consent was received from participants before inclusion in the study. The sample size for each experimental group (n) is indicated in the figure legends and varied between at least three and nine mice/hepatocyte samples per experimental group. For mouse and human models, mice were randomized to each group, and IF/IHC analyses were performed blinded. All in vivo experiments were replicated three or more times by two experimentalists working independently.

Clinical liver transplant study

The recipient and donor variables of the clinical cohort are shown (Tables S1A/B). Study data were collected and managed using REDCap electronic data capture tools hosted at UCLA. All donor organs were perfused and stored in cold UW solution (ViaSpan; Bristol-Meyers Squibb, Garden City, NY). Cold ischemia time was defined as the time from perfusion of the donor organ with UW solution to the removal of the liver from cold storage. Protocol Tru-Cut needle biopsies (Bx) were obtained intra-operatively from the left lobe at about 2h after portal reperfusion (prior to surgical closing of the abdomen) and snap-frozen. A Clavien Dindo Classification system was used to rank the severity of a surgical complication in liver biopsies. It is based on the type of therapy needed to correct the complication. The scale consists of several grades and in this study, Grade III was used to indicate that surgical intervention was necessary. The primer sequences are listed in Table S6 found in (6). The expression of the target gene was normalized to the housekeeping gene, *β-ACT* or *GAPDH* (60).

Statistical analysis

Raw data for experiments in which n < 20 are presented in Data File S1. GraphPad Prism 8.0.1 was used for statistical analyses where SEM represents the mean value SD quotient relative to the square root of N. For mouse experiments, comparisons between two groups or multiple groups were assessed using a two-tailed Student’s t-test, one or two-way analysis of variance ANOVA. A Kruskal-Wallis test or Mann-Whitney U test was used as a nonparametric (distribution free) test. Post-hoc analyses were performed using Dunn’s multiple comparison test or Tukey’s HSD (honest significant difference test), where test assumptions for normality were satisfied by a Shapiro-Wilk or Kolmogorov-Smirnov test. Survival curves were compared using log-rank tests. For human data, continuous values were analyzed by two-tailed Student’s t test, and Fisher’s exact test was

used to determine nonrandom associations between two categorical variables. Spearman's correlation coefficient (r) was used to evaluate the strength of the linear relationship between variables. The cumulative graft survival rate was analyzed by Kaplan-Meier method. A p-value of <0.05 was considered statistically significant.

Supplementary Material

Refer to Web version on PubMed Central for supplementary material.

ACKNOWLEDGMENTS

We thank D. Gjertson of the Department of Pathology and Laboratory Medicine, UCLA, for statistical analyses assistance, John Moulton of Gene-Tools for design of morpholino optimization, J. Shively and M. Kujawski, both City of Hope, for antibody 229 and HepG2 cells. We also thank A. Dery for his summer internship work and TUNEL staining experiments.

Funding:

This work was supported by NIH Grants P01 AI120944 (JWKW), R01 DK062357 (JWKW), DK107533 (JWKW), and DK102110 (JWKW); R01 AI155856-01 (JWKW), NIH Grants R01HL154720 (HKE), R01DK122796 (HKE), R01HL133900 (HKE) and Department of Defense Grant W81XWH2110032 (HKE); NIH Grant R01HL155950 (XY), Parker B. Francis Fellowship (XY), and American Lung Association Catalyst Award CA-622265 (XY).

Data and materials availability:

All data associated with this study are present in the paper or the Supplementary Materials. Mouse strains for OLT study were provided by S. Najjar under an MTA with Ohio University.

References Cited

1. Webster NJG, Alternative RNA Splicing in the Pathogenesis of Liver Disease. Front Endocrinol (Lausanne) 8, 133 (2017). [PubMed: 28680417]
2. Han SP, Tang YH, Smith R, Functional diversity of the hnRNPs: past, present and perspectives. Biochem J 430, 379–392 (2010). [PubMed: 20795951]
3. Geuens T, Bouhy D, Timmerman V, The hnRNP family: insights into their role in health and disease. Hum Genet 135, 851–867 (2016). [PubMed: 27215579]
4. Yeo G, Holste D, Kreiman G, Burge CB, Variation in alternative splicing across human tissues. Genome Biol 5, R74 (2004). [PubMed: 15461793]
5. Wong RJ, Singal AK, Trends in Liver Disease Etiology Among Adults Awaiting Liver Transplantation in the United States, 2014–2019. JAMA Netw Open 3, e1920294 (2020). [PubMed: 32022875]
6. Nakamura K, Kageyama S, Kaldas FM, Hirao H, Ito T, Kadono K, Dery KJ, Kojima H, Gjertson DW, Sosa RA, Kujawski M, Busuttil RW, Reed EF, Kupiec-Weglinski JW, Hepatic CEACAM1 expression indicates donor liver quality and prevents early transplantation injury. J Clin Invest 130, 2689–2704 (2020). [PubMed: 32027621]
7. Dery KJ, Kujawski M, Grunert D, Wu X, Ngyuen T, Cheung C, Yim JH, Shively JE, IRF-1 regulates alternative mRNA splicing of carcinoembryonic antigen-related cell adhesion molecule 1 (CEACAM1) in breast epithelial cells generating an immunoreceptor tyrosine-based inhibition motif (ITIM) containing isoform. Mol Cancer 13, 64 (2014). [PubMed: 24650050]
8. Dery KJ, Gaur S, Gencheva M, Yen Y, Shively JE, Gaur RK, Mechanistic control of carcinoembryonic antigen-related cell adhesion molecule-1 (CEACAM1) splice isoforms by the heterogeneous nuclear ribonuclear proteins hnRNP L, hnRNP A1, and hnRNP M. J Biol Chem 286, 16039–16051 (2011). [PubMed: 21398516]

9. Najjar SM, Accili D, Philippe N, Jernberg J, Margolis R, Taylor SI, pp120/ecto-ATPase, an endogenous substrate of the insulin receptor tyrosine kinase, is expressed as two variably spliced isoforms. J Biol Chem 268, 1201–1206 (1993). [PubMed: 8380406]
10. Dankner M, Gray-Owen SD, Huang YH, Blumberg RS, Beauchemin N, CEACAM1 as a multi-purpose target for cancer immunotherapy. Oncoimmunology 6, e1328336 (2017). [PubMed: 28811966]
11. Nagaishi T, Chen Z, Chen L, Iijima H, Nakajima A, Blumberg RS, CEACAM1 and the regulation of mucosal inflammation. Mucosal Immunol 1 Suppl 1, S39–42 (2008). [PubMed: 19079227]
12. Kim WM, Huang YH, Gandhi A, Blumberg RS, CEACAM1 structure and function in immunity and its therapeutic implications. Semin Immunol 42, 101296 (2019). [PubMed: 31604530]
13. Dery KJ, Silver C, Yang L, Shively JE, Interferon regulatory factor 1 and a variant of heterogeneous nuclear ribonucleoprotein L coordinately silence the gene for adhesion protein CEACAM1. J Biol Chem 293, 9277–9291 (2018). [PubMed: 29720400]
14. Ergun S, Kilik N, Ziegeler G, Hansen A, Nollau P, Gotze J, Wurmbach JH, Horst A, Weil J, Fernando M, Wagener C, CEA-related cell adhesion molecule 1: a potent angiogenic factor and a major effector of vascular endothelial growth factor. Mol Cell 5, 311–320 (2000). [PubMed: 10882072]
15. Chen WJ, Chen HW, Yu SL, Huang CH, Wang TD, Chen JJ, Chien CT, Chen HY, Yang PC, Lee YT, Gene expression profiles in hypoxic preconditioning using cDNA microarray analysis: altered expression of an angiogenic factor, carcinoembryonic antigen-related cell adhesion molecule 1. Shock 24, 124–131 (2005). [PubMed: 16044082]
16. Zwacka RM, Zhang Y, Halldorson J, Schlossberg H, Dudus L, Engelhardt JF, CD4(+) T-lymphocytes mediate ischemia/reperfusion-induced inflammatory responses in mouse liver. J Clin Invest 100, 279–289 (1997). [PubMed: 9218504]
17. Banan B, Xiao Z, Watson R, Xu M, Jia J, Upadhya GA, Mohanakumar T, Lin Y, Chapman W, Novel strategy to decrease reperfusion injuries and improve function of cold-preserved livers using normothermic ex vivo liver perfusion machine. Liver Transpl 22, 333–343 (2016). [PubMed: 26439190]
18. Dery KJ, Nakamura K, Kadono K, Hirao H, Kageyama S, Ito T, Kojima H, Kaldas FM, Busuttil RW, Kupiec-Weglinski JW, Human Antigen R (HuR): A Regulator of Heme Oxygenase-1 Cytoprotection in Mouse and Human Liver Transplant Injury. Hepatology 72, 1056–1072 (2020). [PubMed: 31879990]
19. Yan G, Sun R, Chen Z, Pan X, Sheng Z, Tang C, PTBP1 Targets ILK to Regulate the Hypoxia-Induced Phenotypic Transformation of Pulmonary Artery Smooth Muscle Cells. Drug Des Devel Ther 15, 2025–2033 (2021).
20. Farina AR, Cappabianca L, Sebastiano M, Zelli V, Guadagni S, Mackay AR, Hypoxia-induced alternative splicing: the 11th Hallmark of Cancer. J Exp Clin Cancer Res 39, 110 (2020). [PubMed: 32536347]
21. Farre D, Roset R, Huerta M, Adsuara JE, Rosello L, Alba MM, Messeguer X, Identification of patterns in biological sequences at the ALGGEN server: PROMO and MALGEN. Nucleic Acids Res 31, 3651–3653 (2003). [PubMed: 12824386]
22. Dong W, Song E, Song Y, Co-administration of lipopolysaccharide and D-galactosamine induces genotoxicity in mouse liver. Sci Rep 11, 1733 (2021). [PubMed: 33462304]
23. Tohme S, Geller DA, CEACAM1 and molecular signaling pathways to expand the liver transplant donor pool. J Clin Invest 130, 2192–2194 (2020). [PubMed: 32310220]
24. Xie Q, Chen X, Xu Y, Liang J, Wang F, Liu J, CEACAM1 resists hypoxia-induced inhibition of tube formation of human dermal lymphatic endothelial cells. Cell Signal 45, 145–152 (2018). [PubMed: 29427637]
25. Beauchemin N, Arabzadeh A, Carcinoembryonic antigen-related cell adhesion molecules (CEACAMs) in cancer progression and metastasis. Cancer Metastasis Rev 32, 643–671 (2013). [PubMed: 23903773]
26. Nguyen T, Chen CJ, Shively JE, Phosphorylation of CEACAM1 molecule by calmodulin kinase IID in a three-dimensional model of mammary gland lumen formation. J Biol Chem 289, 2934–2945 (2014). [PubMed: 24302721]

27. Edlund M, Wikstrom K, Toomik R, Ek P, Obrink B, Characterization of protein kinase C-mediated phosphorylation of the short cytoplasmic domain isoform of C-CAM. FEBS Lett 425, 166–170 (1998). [PubMed: 9541029]
28. Chen CJ, Kirshner J, Sherman MA, Hu W, Nguyen T, Shively JE, Mutation analysis of the short cytoplasmic domain of the cell-cell adhesion molecule CEACAM1 identifies residues that orchestrate actin binding and lumen formation. J Biol Chem 282, 5749–5760 (2007). [PubMed: 17192268]
29. Yokoyama S, Chen CJ, Nguyen T, Shively JE, Role of CEACAM1 isoforms in an in vivo model of mammary morphogenesis: mutational analysis of the cytoplasmic domain of CEACAM1–4S reveals key residues involved in lumen formation. Oncogene 26, 7637–7646 (2007). [PubMed: 17546042]
30. Powell DW, Mifflin RC, Valentich JD, Crowe SE, Saada JI, West AB, Myofibroblasts. II. Intestinal subepithelial myofibroblasts. Am J Physiol 277, C183–201 (1999). [PubMed: 10444394]
31. Abrass CK, Berfield AK, Stehman-Breen C, Alpers CE, Davis CL, Unique changes in interstitial extracellular matrix composition are associated with rejection and cyclosporine toxicity in human renal allograft biopsies. Am J Kidney Dis 33, 11–20 (1999). [PubMed: 9915262]
32. Mueller AR, Platz KP, Gebauer B, Schmidt C, Keck H, Lobeck H, Neuhaus P, Changes at the extracellular matrix during acute and chronic rejection in human liver transplantation. Transpl Int 11 Suppl 1, S377–382 (1998). [PubMed: 9665020]
33. Coito AJ, Brown LF, Peters JH, Kupiec-Weglinski JW, van de Water L, Expression of fibronectin splicing variants in organ transplantation: a differential pattern between rat cardiac allografts and isografts. Am J Pathol 150, 1757–1772 (1997). [PubMed: 9137099]
34. Tamkun JW, Schwarzbauer JE, Hynes RO, A single rat fibronectin gene generates three different mRNAs by alternative splicing of a complex exon. Proc Natl Acad Sci U S A 81, 5140–5144 (1984). [PubMed: 6089177]
35. Coito AJ, Binder J, de Sousa M, Kupiec-Weglinski JW, The expression of extracellular matrix proteins during accelerated rejection of cardiac allografts in sensitized rats. Transplantation 57, 599–605 (1994). [PubMed: 8116048]
36. Hide D, Ortega-Ribera M, Garcia-Pagan JC, Peralta C, Bosch J, Gracia-Sancho J, Effects of warm ischemia and reperfusion on the liver microcirculatory phenotype of rats: underlying mechanisms and pharmacological therapy. Sci Rep 6, 22107 (2016). [PubMed: 26905693]
37. Zhai Y, Busuttil RW, Kupiec-Weglinski JW, Liver ischemia and reperfusion injury: new insights into mechanisms of innate-adaptive immune-mediated tissue inflammation. Am J Transplant 11, 1563–1569 (2011). [PubMed: 21668640]
38. Ichijo H, Nishida E, Irie K, ten Dijke P, Saitoh M, Moriguchi T, Takagi M, Matsumoto K, Miyazono K, Gotoh Y, Induction of apoptosis by ASK1, a mammalian MAPKKK that activates SAPK/JNK and p38 signaling pathways. Science (New York, N.Y.) 275, 90–94 (1997). [PubMed: 8974401]
39. Kirshner J, Chen CJ, Liu P, Huang J, Shively JE, CEACAM1–4S, a cell-cell adhesion molecule, mediates apoptosis and reverts mammary carcinoma cells to a normal morphogenic phenotype in a 3D culture. Proc Natl Acad Sci U S A 100, 521–526 (2003). [PubMed: 12522268]
40. Iversen PL, Arora V, Acker AJ, Mason DH, Devi GR, Efficacy of antisense morpholino oligomer targeted to c-myc in prostate cancer xenograft murine model and a Phase I safety study in humans. Clin Cancer Res 9, 2510–2519 (2003). [PubMed: 12855625]
41. Karaki S, P. C., R. P., in Antisense Therapy. (IntechOpen, 2019).
42. Sena JA, Wang L, Heasley LE, Hu CJ, Hypoxia regulates alternative splicing of HIF and non-HIF target genes. Mol Cancer Res 12, 1233–1243 (2014). [PubMed: 24850901]
43. Stoehr A, Yang Y, Patel S, Evangelista AM, Aponte A, Wang G, Liu P, Boylston J, Kloner PH, Lin Y, Gucek M, Zhu J, Murphy E, Prolyl hydroxylation regulates protein degradation, synthesis, and splicing in human induced pluripotent stem cell-derived cardiomyocytes. Cardiovasc Res 110, 346–358 (2016). [PubMed: 27095734]
44. Chang SH, Elemento O, Zhang J, Zhuang ZW, Simons M, Hla T, ELAVL1 regulates alternative splicing of eIF4E transporter to promote postnatal angiogenesis. Proc Natl Acad Sci U S A 111, 18309–18314 (2014). [PubMed: 25422430]

45. Williams AL, Walton CB, Pinell B, Khadka VS, Dunn B, Lee K, Anagaran MCT, Avelar A, Shohet RV, Ischemic heart injury leads to HIF1-dependent differential splicing of CaMK2γ. Scientific Reports 11, 13116 (2021). [PubMed: 34162925]
46. Duan C, Hypoxia-inducible factor 3 biology: complexities and emerging themes. Am J Physiol Cell Physiol 310, C260–269 (2016). [PubMed: 26561641]
47. Zhang J, Qin Y, Martinez M, Flores-Bellver M, Rodrigues M, Dinabandhu A, Cao X, Deshpande M, Qin Y, Aparicio-Domingo S, Rui Y, Tzeng SY, Salman S, Yuan J, Scott AW, Green JJ, Canto-Soler MV, Semenza GL, Montaner S, Sodhi A, HIF-1α and HIF-2α redundantly promote retinal neovascularization in patients with ischemic retinal disease. J Clin Invest 131, (2021).
48. Peng T, Du SY, Son M, Diamond B, HIF-1α is a negative regulator of interferon regulatory factors: Implications for interferon production by hypoxic monocytes. Proc Natl Acad Sci U S A 118, (2021).
49. Liu Y, Gonzàlez-Porta M, Santos S, Brazma A, Marioni JC, Aebersold R, Venkitaraman AR, Wickramasinghe VO, Impact of Alternative Splicing on the Human Proteome. Cell Rep 20, 1229–1241 (2017). [PubMed: 28768205]
50. Dengler VL, Galbraith M, Espinosa JM, Transcriptional regulation by hypoxia inducible factors. Crit Rev Biochem Mol Biol 49, 1–15 (2014). [PubMed: 24099156]
51. Kular D, Macdougall IC, HIF stabilizers in the management of renal anemia: from bench to bedside to pediatrics. Pediatr Nephrol 34, 365–378 (2019). [PubMed: 29569190]
52. Zhdanov AV, Okkelman IA, Collins FW, Melgar S, Papkovsky DB, A novel effect of DMOG on cell metabolism: direct inhibition of mitochondrial function precedes HIF target gene expression. Biochim Biophys Acta 1847, 1254–1266 (2015). [PubMed: 26143176]
53. Kato S, Takahashi T, Miyata N, Roman RJ, DMOG, a Prolyl Hydroxylase Inhibitor, Increases Hemoglobin Levels without Exacerbating Hypertension and Renal Injury in Salt-Sensitive Hypertensive Rats. J Pharmacol Exp Ther 372, 166–174 (2020). [PubMed: 31801803]
54. Yu J, Sun G, Chen Y, Li L, Wang H, Tu D, Li L, Meng Z, Wang Y, CEACAM1 Inhibited IκB-α/NF-κB Signal Pathway Via Targeting MMP-9/TIMP-1 Axis in Diabetic Atherosclerosis. J Cardiovasc Pharmacol 76, 329–336 (2020). [PubMed: 32569018]
55. Schelter F, Halbgewachs B, Bäumler P, Neu C, Görlach A, Schrötzlmair F, Krüger A, Tissue inhibitor of metalloproteinases-1-induced scattered liver metastasis is mediated by hypoxia-inducible factor-1α. Clin Exp Metastasis 28, 91–99 (2011). [PubMed: 21053058]
56. Sripariwuth E, Piwchan S, Pongcharoen S, Serum Carcinoembryonic Antigen-Related Cell Adhesion Molecule 1 Level in Patients with Hepatocellular Carcinoma. Asian Pac J Cancer Prev 22, 3521–3524 (2021). [PubMed: 34837908]
57. Kim SG, Ahn SY, Lee ES, Kim S, Na KY, Chae DW, Chin HJ, Bilirubin activates transcription of HIF-1α in human proximal tubular cells cultured in the physiologic oxygen content. J Korean Med Sci 29 Suppl 2, S146–154 (2014). [PubMed: 25317019]
58. Kochhar G, Parungao JM, Hanouneh IA, Parsi MA, Biliary complications following liver transplantation. World J Gastroenterol 19, 2841–2846 (2013). [PubMed: 23704818]
59. Hirao H, Kojima H, Dery KJ, Nakamura K, Kadono K, Zhai Y, Farmer DG, Kaldas FM, Kupiec-Weglinski JW, Neutrophil CEACAM1 determines susceptibility to NETosis by regulating the S1PR2/S1PR3 axis in liver transplantation. J Clin Invest 133, (2023).
60. Kadono K, Dery KJ, Hirao H, Ito T, Kageyama S, Nakamura K, Oncel D, Aziz A, Kaldas FM, Busuttil RW, Kupiec-Weglinski JW, Heme Oxygenase-1 dictates innate - adaptive immune phenotype in human liver transplantation. Arch Biochem Biophys 671, 162–166 (2019). [PubMed: 31299184]
61. Blau DM, Turbide C, Tremblay M, Olson M, Létourneau S, Michaliszyn E, Jothy S, Holmes KV, Beauchemin N, Targeted disruption of the Ceacam1 (MHVR) gene leads to reduced susceptibility of mice to mouse hepatitis virus infection. J Virol 75, 8173–8186 (2001). [PubMed: 11483763]
62. Al-Share QY, DeAngelis AM, Lester SG, Bowman TA, Ramakrishnan SK, Abdallah SL, Russo L, Patel PR, Kaw MK, Raphael CK, Kim AJ, Heinrich G, Lee AD, Kim JK, Kulkarni RN, Philbrick WM, Najjar SM, Forced Hepatic Overexpression of CEACAM1 Curtails Diet-Induced Insulin Resistance. Diabetes 64, 2780–2790 (2015). [PubMed: 25972571]

63. Russo L, Muturi HT, Ghadieh HE, Ghanem SS, Bowman TA, Noh HL, Dagdeviren S, Dogbey GY, Kim JK, Heinrich G, Najjar SM, Liver-specific reconstitution of CEACAM1 reverses the metabolic abnormalities caused by its global deletion in male mice. Diabetologia 60, 2463–2474 (2017). [PubMed: 28913658]

64. Ghadieh HE, Russo L, Muturi HT, Ghanem SS, Manaserh IH, Noh HL, Suk S, Kim JK, Hill JW, Najjar SM, Hyperinsulinemia drives hepatic insulin resistance in male mice with liver-specific Ceacam1 deletion independently of lipolysis. Metabolism 93, 33–43 (2019). [PubMed: 30664851]

65. Guide for the Care and Use of Laboratory Animals. (National Academies Press, 2011).

66. Nakamura K, Zhang M, Kageyama S, Ke B, Fujii T, Sosa RA, Reed EF, Datta N, Zarrinpar A, Busuttil RW, Araujo JA, Kupiec-Weglinski JW, Macrophage heme oxygenase-1-SIRT1-p53 axis regulates sterile inflammation in liver ischemia-reperfusion injury. J Hepatol 67, 1232–1242 (2017). [PubMed: 28842295]

67. Kadono K, Kageyama S, Nakamura K, Hirao H, Ito T, Kojima H, Dery KJ, Li X, Kupiec-Weglinski JW, Myeloid Ikaros-SIRT1 signaling axis regulates hepatic inflammation and pyroptosis in ischemia-stressed mouse and human liver. J Hepatol 76, 896–909 (2022). [PubMed: 34871625]

68. Shen XD, Gao F, Ke B, Zhai Y, Lassman CR, Tsuchihashi S, Farmer DG, Busuttil RW, Kupiec-Weglinski JW, Inflammatory responses in a new mouse model of prolonged hepatic cold ischemia followed by arterialized orthotopic liver transplantation. Liver Transpl 11, 1273–1281 (2005). [PubMed: 16184555]

69. Tamaki N, Hatano E, Taura K, Tada M, Kodama Y, Nitta T, Iwaisako K, Seo S, Nakajima A, Ikai I, Uemoto S, CHOP deficiency attenuates cholestasis-induced liver fibrosis by reduction of hepatocyte injury. Am J Physiol Gastrointest Liver Physiol 294, G498–505 (2008). [PubMed: 18174271]

70. Suzuki S, Toledo-Pereyra LH, Rodriguez FJ, Cejalvo D, Neutrophil infiltration as an important factor in liver ischemia and reperfusion injury. Modulating effects of FK506 and cyclosporine. Transplantation 55, 1265–1272 (1993). [PubMed: 7685932]

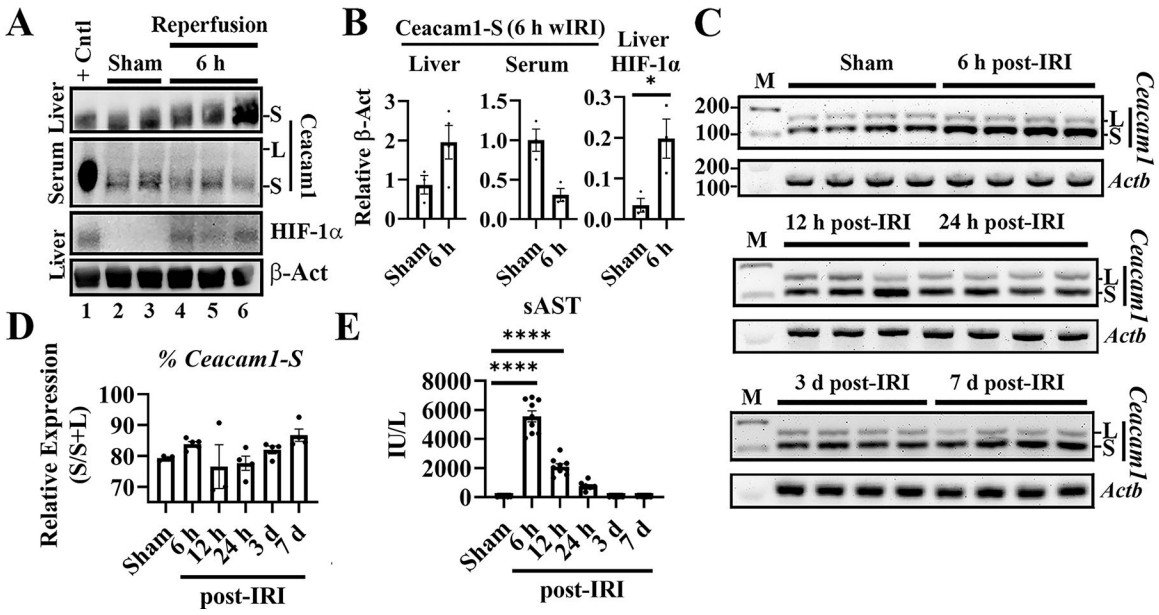

Fig. 1. Acute liver injury promotes *Ceacam1* alternative splicing (AS).

(A) Western blots of Ceacam1 and Hif-1α from livers and serum isolated from C57BL/6 mice subjected to wIRI at time-points 0 h (Sham) vs. 6h post-reperfusion. **(B)** Quantitation of hepatic Ceacam1 and Hif-1α expression from panel A, relative to β-Act (n=3–4/group). Hif-1α Sham vs. 6h by unpaired Student's t-test (P=0.0324). **(C)** Total mRNAs were subjected to exon junction primers designed to measure each splice variant. M is marker with sizes (bp) shown on the left and L and S denote *Ceacam1-L* or *Ceacam1-S*, respectively. Biological replicates/group are represented by black line above each blot. **(D)** Quantitation of % *Ceacam1-S* relative to total *Ceacam1* mRNA from panel D was analyzed by Kruskal-Wallis test (P<0.034; n=3–4/group). **(E)** Serum AST (sAST) was analyzed by one-way ANOVA (P<0.0001). IU/L is International Units Per Liter. Tukey's HSD test for Sham vs. 6h and Sham vs. 12h were both P<0.0001. For panels B-D, Sham, *Actb*, and β-Act served as internal controls. Data shown are mean±SEM, using at least n=3–9/group.

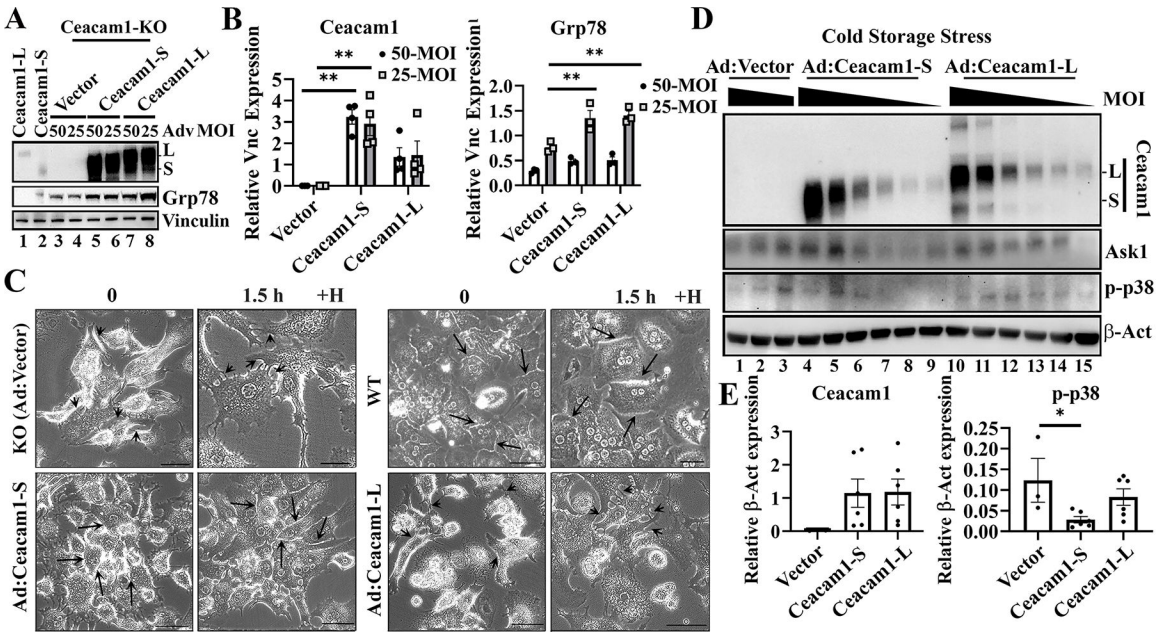

Fig. 2. Ad: Ceacam1-S rescues hypoxia-triggered cellular stress in murine hepatocytes through Ask1/p-p38 signaling.

(A) Ceacam1-deficient (KO) mouse hepatocytes were transfected with Ad-viral particles at the indicated MOI (multiplicity of infection). WT lysates (+) show endogenous amounts. **(B)**. Quantitation of Ad: Ceacam1 isoforms and Grp78 protein expression from 50 vs. 25 MOI lysates were analyzed by two-way ANOVA for both groups (P<0.0001, Ceacam1; P=0.0005, Grp78), followed by Tukey's HSD. Expression was relative to internal standard Vnc (n=3–4/group). **(C)** Bright-field microscopy of Ad-expressing hepatocytes treated with hypoxia (+H) for the indicated time. Black arrows indicate areas of cellular adhesion, whereas black arrowheads show lack thereof. Representative specimens (n=3/group; all images were 125–150 x original magnification except for 0 x for WT -H, scale bar shows 100 μm). Representative specimens (n=3/group; original magnification ×160, scale bar shows 100 μm). **(D)** Viruses were given undiluted (lanes 1, 4, 10) or diluted 1/2 (lanes 2, 5, 11), 1/5 (lanes 3, 6, 12), 1/10 (lanes 7, 13), 1/20 (lanes 8, 14), and 1/40 (lanes 9, 15) MOI concentration as denoted by the descending black triangle. Western blots were evaluated for protein expression of Ceacam1, Ask1, p-p38 and β-Act (n=3–6/group). **(E)** Quantification of data from panel D. A Kruskal-Wallis test was used for parallel p-p38 samples (P=0.0235) relative to β-Act (n=3–6/group). The collective set of MOIs were grouped for Ceacam1 and p-p38 analyses. Post-hoc analyses were performed using an uncorrected Dunn's test (P=0.0177). Data shown are mean±SEM and represent at least three biological replicates. *, ** represent P values <0.05 and <0.01.

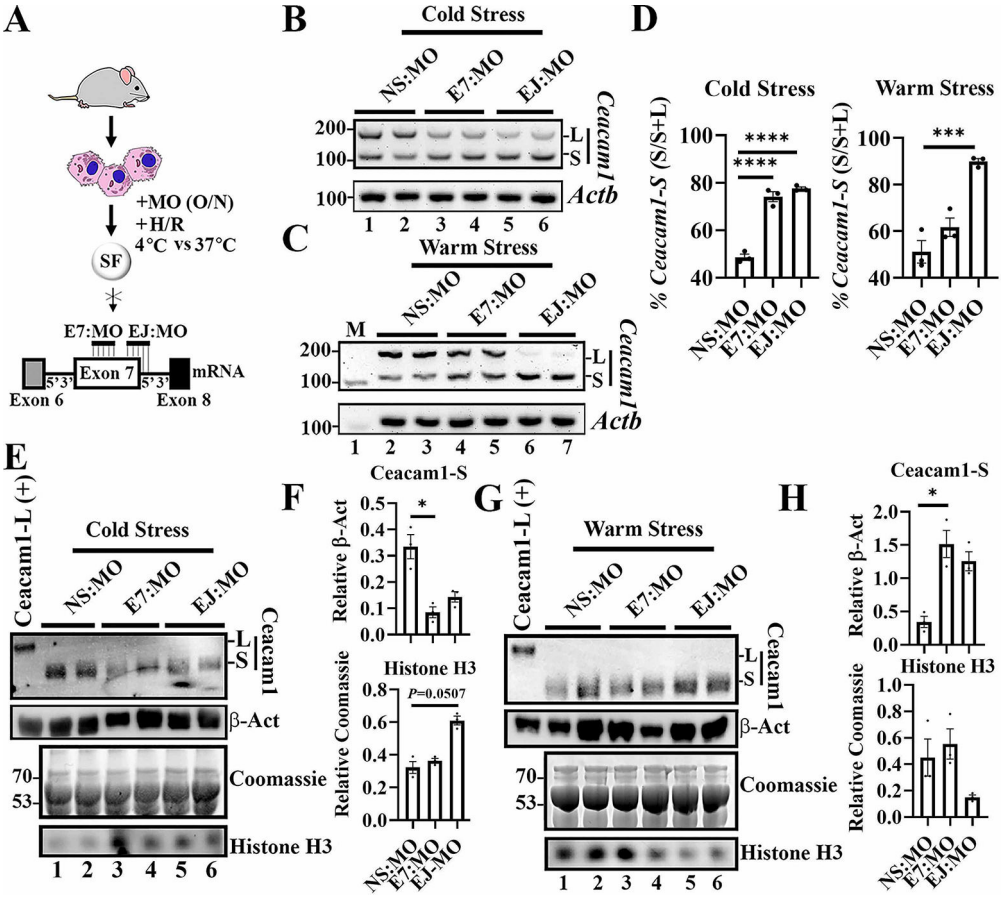

Fig. 3. Induction of AS of *Ceacam1* by splice-blocking morpholino oligomers (MOs) protects murine hepatocytes against temperature-induced stress in vitro.

(A) Experimental scheme targeting variable exon 7 using morpholinos (MO) under hypoxia-reoxygenation (H/R) stimulation (see Supplemental Materials for more details). **(B-C)** Exon-junction RT-PCR of *Ceacam1* isoforms in cold storage stress (4°C) vs. warm storage stress (37°C) conditions, (n=3/group). L and S notations mark isoform positions, and *Actb* is the loading control. **(D)** Quantification of *Ceacam1-S* expression based on panels B-C data. Expression normalized to total *Ceacam1* mRNA. One-way ANOVA analyses for cold and warm storage stress MO groups (P=0.0001 and P=0.0008) was followed by Tukey's HSD test for EJ:MO or E7:MO vs. NS:MO cold storage stress samples (P<0.0001 each) and for EJ:MO vs. NS:MO warm storage stress samples (P<0.0007). **(E, G)** Western blot detection for Ceacam1, β-actin and histone H3 under cold stress (panel E) vs. warm stress (panel G). Coomassie staining was also performed to normalize histone H3 expression. **(F, H)** Quantification of protein data from panels E and G. Expression normalized to β-actin and Coomassie stain. A Kruskal-Wallis test was used for cold and warm storage stress Ceacam1 MO groups (P=0.0107 and P=0.0250) were followed by Tukey's HSD test for E7:MO vs. NS:MO cold storage stress samples (P<0.0225) and E7:MO vs. NS:MO warm storage stress samples (P<0.0341), (n=3/group). Histone H3 served as an indicator of hepatocellular stress. Data shown are mean±SEM and represent at least three biological replicates. ***, ***, ****** represent P values <0.05, <0.001, and <0.0001, respectively, for differences between groups.

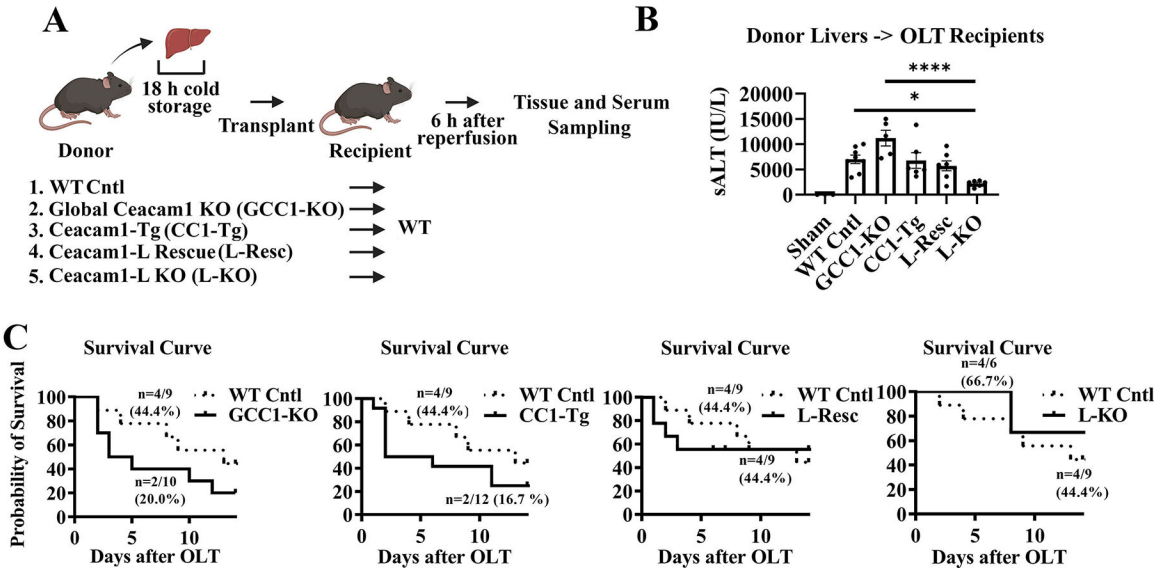

Fig. 4. Hepatic Ceacam1-L exacerbates liver IRI and reduces OLT survival.

(A) Genetically modified mouse (C57BL/6) donor livers, subjected to extended cold storage (18h), were transplanted to syngeneic WT recipients. Donors were characterized by: Global Ceacam1 deficiency (GCC1-KO, n=10); liver-specific rat Ceacam1-L overexpression in the C57BL/6 background (CC1-Tg; n=9), or the Global Ceacam1-KO background (L-Resc, n=9); and liver-specific Ceacam1-L deficiency (L-KO, n=9). **(B)** Serum was collected 6h post-reperfusion for ALT analyses (IU/L, n=3–8/group). Ordinary one-way ANOVA analyses of donor liver groups (P=0.0001) were followed by Tukey's HSD test for WT Control (Cntl) vs. L-KO (P=0.0250) and GCC1-KO vs. L-KO (P<0.0001). **(C)** Animals were monitored for 14 days, and cumulative survival rates were estimated using the Kaplan-Meier method. Survival curves were compared using log-rank tests where the calculated observed number of deaths in each group was compared to the number expected if there were no differences between the groups. The dotted line indicates WT controls (n=9), while the solid indicates Ceacam1 experimental groups.

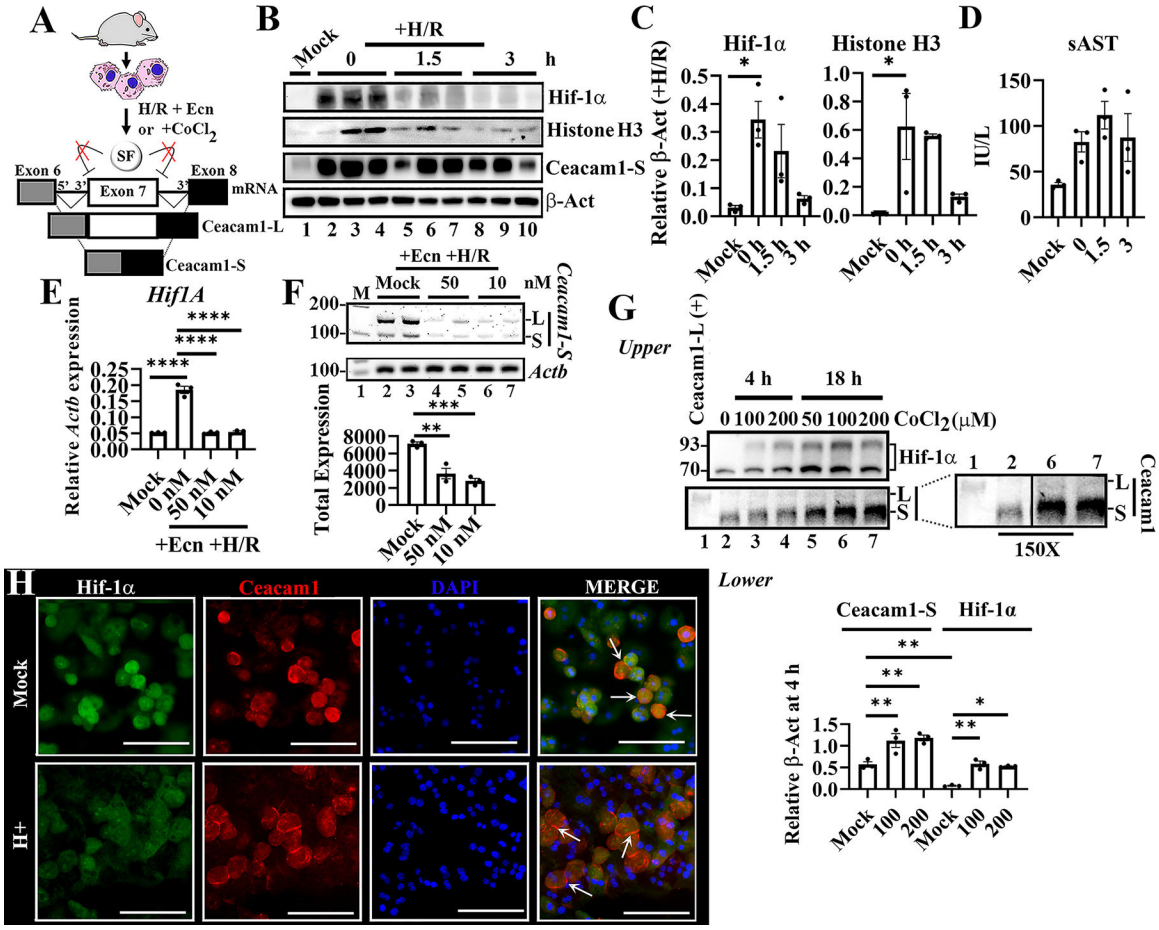

Fig. 5. Hif-1α influences pre-and post-transcriptional Ceacam1 expression in murine hepatocytes in vitro.

(A) Experimental scheme using inhibitor Echinomycin (Ecn) or stabilizer ($CoCl_2$) of Hif-1α in oxygen-stress conditions. **(B)** Time course of Hif-1α, Ceacam1-S, and histone H3 expression with hypoxia followed by indicated periods of normoxia. **(C)** Quantitation of histone H3 and Hif-1α from parallel panel B samples, measured by one-way ANOVA Kruskal Wallis test [Hif-1α (P<0.0139), histone H3 (P<0.0197) mock vs. 0 h]. **(D)** Quantitation of AST levels from culture media collected from panel B samples. **(E)** qRT-PCR detection of mRNA coding for *Hif-1α* relative *Actb* expression. **(F)** Exon junction RT-PCR and quantification for *Ceacam1* isoforms and *Actb* analyzed by one-way ANOVA (P=0.00023, P=0.0007, mock vs. 50 and 10 nM) **(G)** Western blot of cultured normoxic hepatocytes treated with $CoCl_2$ for either 4h or 18h (*upper)* panel. Magnified lanes highlight the production of Ceacam1-L. Positive Ceacam1-L control obtained from mouse intestinal tissue. Quantitation of Ceacam1-S and Hif-1α, relative to β-Act are in *lower* panel. **(H)** Immunofluorescence detection of Hif-1α and Ceacam1 from mouse hepatocytes in vitro exposed to hypoxia for 90min (H+). White arrows indicate cellular Ceacam1 location. Original magnification is x20, scaled upwards 120x for visualization. Scale bar shows 100 μm. Panels C-G were analyzed by one-way ANOVA. Post-hoc analyses for panel C used Dunn's test, whereas panels D-G used Tukey's HSD analyses (at least n=3/group). Data

shown are mean±SEM. ***, **, ***, ****** represent *P* values <0.05, <0.01, <0.001, and <0.0001, respectively.

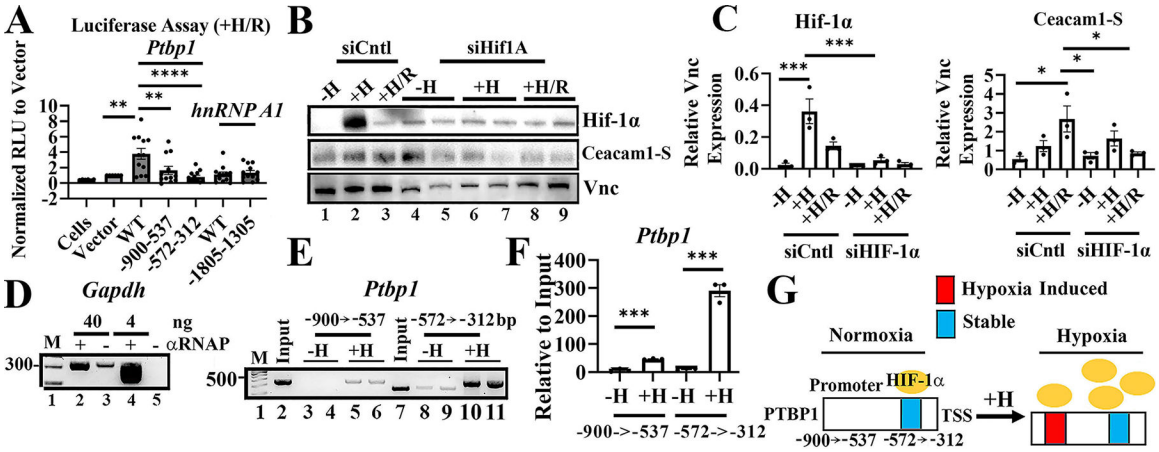

Fig. 6. Hif-1α promotes *Ptbp1* expression during hypoxia.

(A) Luciferase assays determined the relationship between Hif-1α, Ptbp1, and hnRNP A1. WT C57BL/6hepatocytes were transfected with constructs containing either WT or deletion mutations as shown, relative to the transcription start site (TSS), following H/R (n=6–12 biological replicates). Data analyzed by one-way ANOVA followed by Tukey's HSD test. **(B)** Western blotting data for Ceacam1-S, Hif-1α and Vnc after RNA interference of Hif-1α and hypoxia/reoxygenation. Antibodies were directed to Hif-1α, Ceacam1 and Vnc. **(C)** Densitometer quantitation from panel B (n=3) analyzed by one-way ANOVA followed by Tukey's HSD test. Vnc was used for normalization. (**D)** Anti-RNA polymerase II Ab and primers were used with GAPDH as a positive control for ChIP RT-PCR, establishing sensitivity and specificity conditions. Four ng ChIP DNA was used for downstream Ptbp1 studies. **(E)** ChIP of mouse Ptbp1 using antibody directed to Hif-1α. The region of the promoter targeted is notated above the panel. The apparent slower migration of DNA Ptbp1 for region −572 to −312 relative the input is attributed to mass of product loaded, as compared to normoxia samples. **(F)** Quantitation of parallel ChIP Ptbp1 panel E samples. Unpaired Student's t-test of representative samples was performed for −900->−537 ±H (P=0.0002) and −900->−537 ±H (P=0.0002). **(G)** Summary of Hif-1α dependent interactions. Stable interactions were present before and after hypoxia, whereas hypoxia induced interactions occurred only after limited oxygen availability. Data shown are mean±SEM and represent at least three biological replicates. ***, **, ***, ****** represent P values <0.05, <0.01, <0.001, and <0.0001, respectively.

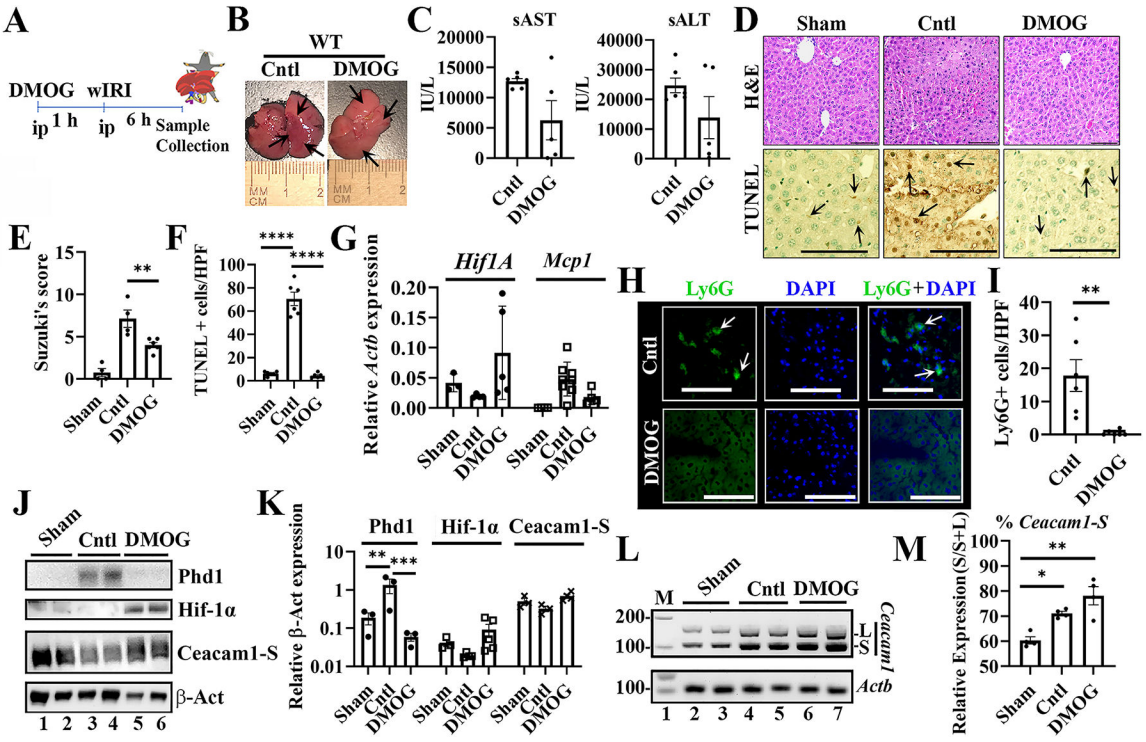

Fig. 7. DMOG alleviates liver injury in mice and promotes *Ceacam1* alternative splicing.

(A) Experimental scheme for wIRI and treatment. **(B)** Gross anatomical examination of Control (Cntl; no DMOG, +wIRI) vs. DMOG (+ treatment +wIRI). Black arrows indicate areas of liver damage or lack thereof. **(C)** sAST (*P*=0.057, unpaired Student's t-test) and sALT concentrations in control and DMOG treated mice (n=5–6/group). **(D)** Representative images of H&E and TUNEL staining (brown) in liver tissue. Black arrows indicate dead cells. Original magnification, x20, scale 1/70). Scale bar shows 100μm. **(E)** Suzuki's histological grading of liver IRI in Sham, control and DMOG treated mice (n=4–6/group). **(F)** Quantification of TUNEL-positive cells from panel D (n=6/HPF). **(G)** qRT-PCR analysis of *Hif1A* and *Mcp1* mRNA expression after normalization to *Actb*. (n=3–8 per group). **(H)** Representative immunohistochemical staining of Ly6G (green) and nuclei (DAPI, blue) in liver tissue from control (Cntl) and DMOG treated mice. Arrows indicate extranuclear staining of $Ly6G^{+}$ cells (original magnification, x20; scale bar shows 100 μm). **(I)** Quantification of infiltrating Ly6G-positive neutrophils/6HPF. **(J)** Western blots and **(K)** relative intensity ratios of PhD1, Hif-1α, and Ceacam1 expression in Sham, control and DMOG treated livers, (n=3–5/group). **(L)** RT-PCR to measure *Ceacam1* splice variant mRNA expression in Sham, control and DMOG treated livers. **(M)** Relative intensity ratios to measure % *Ceacam1-S* in panel L. Panels C and I were analyzed by Mann-Whitney tests whereas panels E-F were analyzed by one-way ANOVA and Tukey's HSD test. Panel G and K were analyzed by two-way ANOVA and Tukey's HSD test. Panel M by Kruskal-Wallis test followed by post-hoc Dunn's test. β-Act served as loading control. Data shown are mean±SEM. ***, **, ***, ****** represent *P* values <0.05, <0.01, <0.001, and <0.0001, respectively.

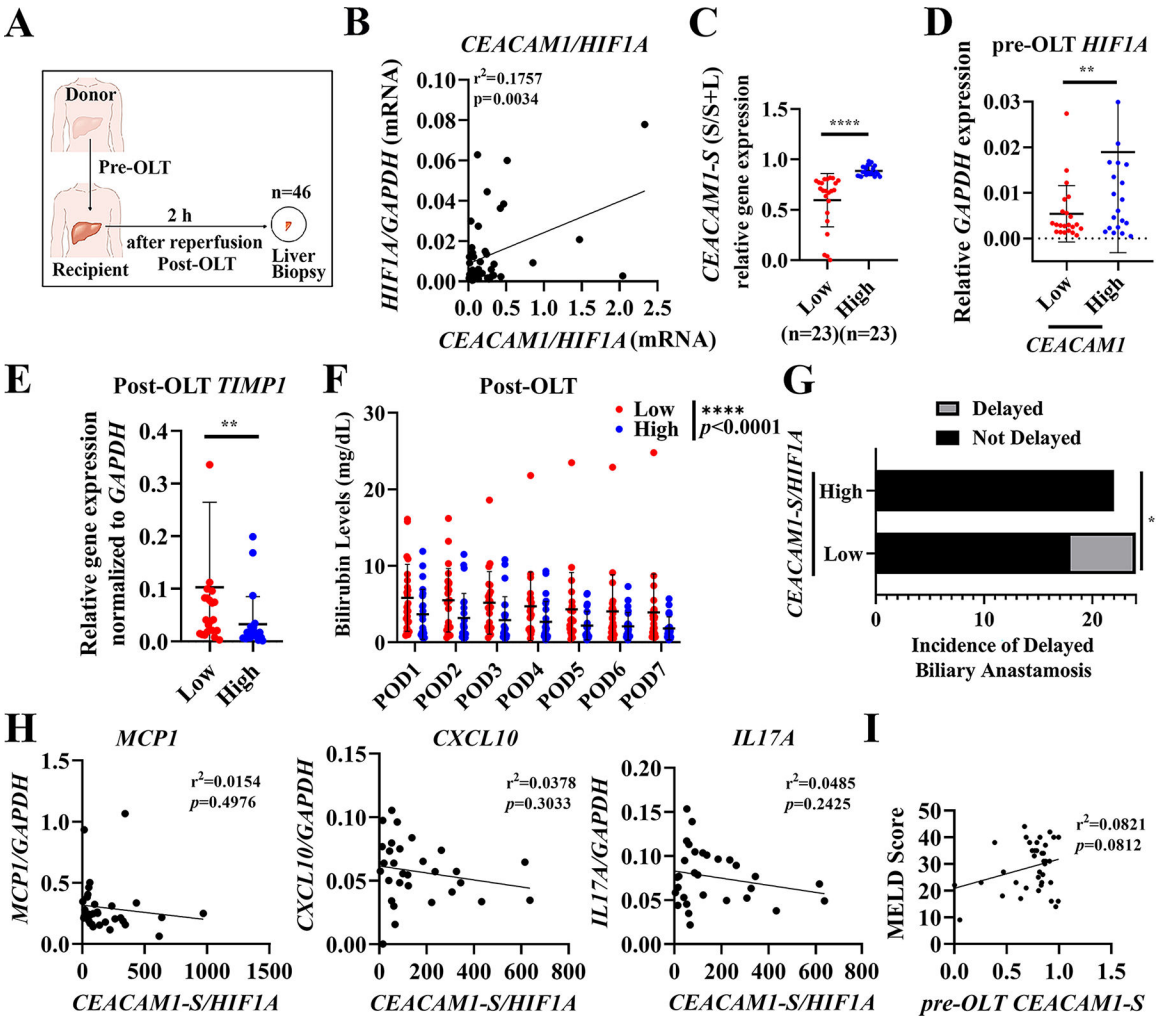

Fig. 8. Hepatic *CEACAM1-S* mRNA expression associates with *HIF1A* mRNA in human OLT recipients before liver implantation.

(A) Forty-six human donor liver biopsies (Bx) were collected before (pre-OLT) and after transplantation (post-OLT). **(B)** Pre-transplant *HIF1A* vs. *CEACAM1-S* mRNA expression by Spearman r analyses. **(C)** Pre-transplant human liver Bx samples were divided into low (n=23; red) and high (n=23; blue) *CEACAM1-S* expression groups, after normalization to *CEACAM1* total mRNA (S/S+L), $P<0.0001$. **(D)** High *CEACAM1-S* expression pre-transplant compared to pre-OLT *HIF1A* expression, $P=0.0080$. **(E-H)** Pre-transplant *CEACAM1-S*/*HIF1A* ratios were compared to post-OLT *TIMP1*, $P=0.0012$ (Mann-Whitney U test). **(F)** Total bilirubin on postoperative day 1 (POD)-POD7, relative *CEACAM1*:*HIF1A* by two-way ANOVA ($P<0.0001$, high vs. low *CEACAM1/HIF-1α*). **(G)** Incidence of delayed biliary anastomosis (Fisher's exact test, $P<0.0223$), relative *CEACAM1-S*/*HIF1A*. **(H)** Correlation of *CEACAM1-S*/*HIF1A* ratios to *MCP1, CXCL10, IL17A* mRNA expression in post-transplant Bx (Spearman r). **(I)** Spearman r analyses for pre-transplant *CEACAM1-S* expression and MELD score.